doi:10.14311/ppt.2025.3.202
Plasma Physics and Technology **12**(3):202–207, 2025

SENSITIVITY OF SYNTHETIC TEST CIRCUIT PARAMETERS ON THERMAL INTERRUPTION TESTS IN CO_2 GAS MIXTURES

D. Kumari*, C. M. Franck

High Voltage Laboratory, ETH Zürich, Physikstrasse 3, 8092, Switzerland

* dkumari@ethz.ch

Abstract. Synthetic testing has been extensively utilized to study the thermal interruption performance of CO_2-based gas mixtures under the influence of varying physical factors in an experimental HV circuit breaker. To limit contact and nozzle ablation for collecting a statistically meaningful dataset, the lowest possible peak current amplitudes were chosen for the high-current and the injection current phases. The present work focuses on evaluating the sensitivity of the test-circuit parameters on the interruption performance in CO_2 /O_2 (90% /10%) gas mixture.

Keywords: blown arc, synthetic testing, SF_6-alternatives, gas circuit breaker.

1. Introduction

Synthetic testing—originally developed as an alternative to direct testing—has become a preferred and cost-effective approach for performing type tests on HV/UHV circuit breakers (CB). This method enables the independent generation of high short-circuit currents and steep recovery voltages (post-current zero), significantly reducing the power required during testing. Synthetic test circuits can closely replicate various grid-fault test duties, such as the L90 and T100 duties specified in international standards [1, 2].

To investigate the current interruption capability in CBs, synthetic test circuits have been extensively employed for research purposes over several decades [3–5]. However, subjecting the experimental CB to high short-circuit currents introduces undesired aging during the course of testing. To address this issue, a current with reduced amplitude was opted at grid frequency in the high-current phase as it was demonstrated that it resulted in the same thermal recovery speed as the experiments with short-circuit currents, consequently, have similar current-zero (CZ) conditions [6].

Leveraging this result, an in-house synthetic circuit is used to obtain statistically 'large' dataset to study the thermal current interruption performance in an experimental puffer-type CB using CO_2-based gas mixtures under varying controlled physical conditions like contact gap distance, blow pressure and gas flow field at the instant of CZ [7–12].

A Weil-Dobke inspired synthetic test circuit generates three distinct stresses at different instants: the high current phase, the injection current phase immediately before CZ, and the transient recovery voltage phase post CZ. The particular stress of the L90 test duty comes from the immediate occurrence of a rate-of-rise of recovery voltage without any time delay, which leads to the so-called thermal interruption challenge.

In this work, the influence of the variation in the severity of these 3 stresses are studied in a CO_2 /O_2 (90% /10%) and gist of the experiments are discussed as follows:

- High-current (HC) phase: The 50 Hz fault current with reduced amplitude flows while the contacts separate, generating a 'stabilized' arc lasting 10 ms. Maintaining the current amplitude close to 2 kA minimizes nozzle ablation and back-heating, thereby keeping the blow pressure fairly constant across consecutive tests. By increasing the amplitude from 2 kA to 5 kA, the sensitivity of this phase on the interruption performance is evaluated.
- Injection current (IC) phase: To control the $\mathrm{d}i/\mathrm{d}t$ slope, a current pulse is injected near the zero-crossing of the high current (HC). In this work, the IC is increased from the 2–3 kA range to the 3–4 kA range, while keeping the same $\mathrm{d}i/\mathrm{d}t$ values, cf. Fig. 1. The moderate and high HC closely follow the short-circuit current at 50 Hz for 100 µs and 170 µs respectively with 5% deviation.
- Transient recovery voltage (TRV) phase: Immediately after CZ, a steeply rising voltage appears whose rate-of-rise (RRRV)$=Z_s \cdot \mathrm{d}i/\mathrm{d}t$ at CZ. Here, the peak of TRV is increased from 30 kV to 36 kV while keeping the $\mathrm{d}u/\mathrm{d}t$ the same to study its influence on the thermal interruption and 'hot-dielectric reignitions' which occur in the thermal phase and exhibit the features of an electric breakdown [10], cf. Fig. 2.

2. Methodology

2.1. Experiment Setup

The device under test is an experimental puffer circuit breaker, tailor-made to achieve controllable and reproducible physical conditions during current interruption tests. The breaker is typically configured to generate a blow pressure of (10.8 ± 0.2) bar, directed into the nozzle inlet and blowing onto the arcing channel. The contact gap is set to (43 ± 1) mm and the

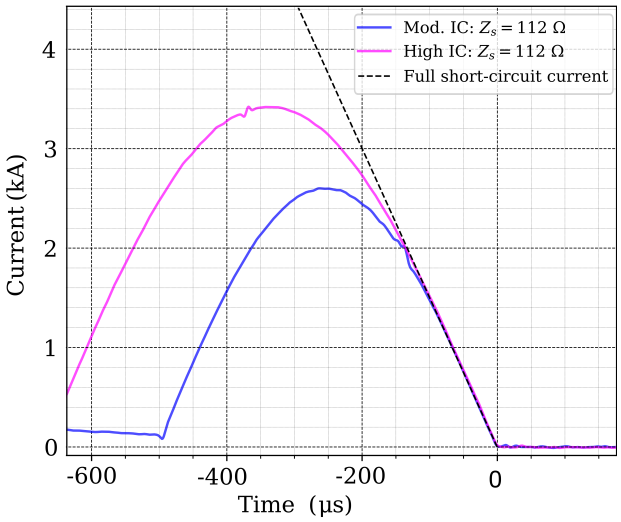

Figure 1. Plot of moderate (Q0) and high injection current (Q1), following the corresponding full short-circuit current at 50 Hz for the last 100 µs and 170 µs respectively before CZ.

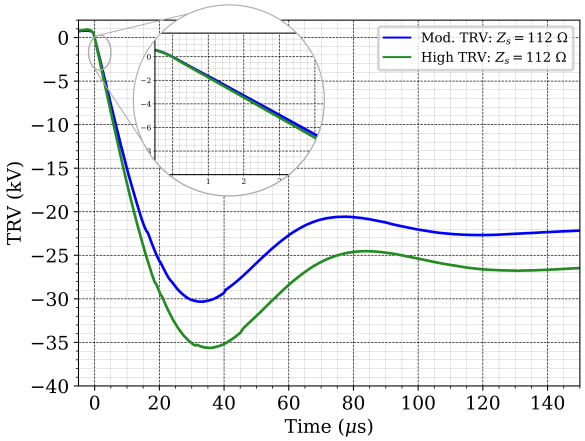

Figure 2. Plot of moderate (Q0) and high transient recovery voltage (Q2) with the similar du/dt *post CZ for 4 µs and TRV delay <100 ns.*

nozzle outlet venting into a vessel maintained at 5 bar (absolute). This blow pressure is sufficient to induce sonic flow at the nozzle throat which is cardinal for arc extinction.

The synthetic circuit (Fig. 3) generates current and voltage stresses similar to SLF L90 fault duty inside the CZ time window, spanning ∼150 µs before CZ to 4 µs after. It incorporates a high-current circuit (HCC) implemented as an LC circuit with a switching element to produce the current at grid frequency during contact opening. In the high-current circuit (HCC), the peak current amplitude is generally maintained at 2 kA to avoid back-heating and minimize nozzle ablation, but has been varied in this study. In parallel, a current injection circuit (CIC) is responsible for generating key CZ quantities - current slope ($\frac{di}{dt}$) and rate-of-rise of recovery voltage, RRRV ($\frac{du}{dt}$). The characteristic surge impedance of the circuit, defined as the ratio $\frac{du}{dt}/\frac{di}{dt}$, is 450 Ω for the L90 fault duty. CIC operates in a regime where the peak current reaches ∼2.5 kA at the expected $\frac{di}{dt}$ limit with an operating frequency of 250 Hz-1000 Hz.

Detailed description of the experiment setup and corresponding test series can be found in works [10–13].

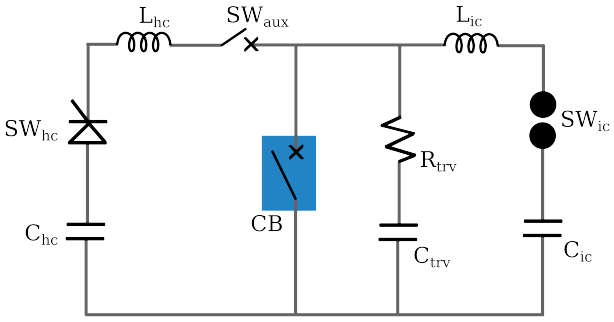

Figure 3. Synthetic circuit topology with high current circuit (HCC) and current injection circuit (CIC) on the left and right of the experimental circuit breaker (blue) respectively

2.2. Injection Circuit Design

The CIC consists of two main branches: a) LC resonant branch, L_{ic} and C_{ic} and b) TRV-shaping branch, R_{trv} and C_{trv}. The capacitor bank, C_{ic} is charged to $U_c \leq 35$ kV. The LC branch generates a sinusoidal current pulse given the desired peak amplitude and initial slope.

At the first zero crossing of the injection current and if the CB interrupted the current, the capacitor in the TRV-shaping branch, C_{trv}, begins to take up charge from C_{ic} through L_{ic} and R_{trv}, resulting in an under-damped voltage waveform that serves as the transient recovery voltage (TRV). The peak TRV value is strongly influenced by the initial charging voltage of C_{ic}, while the rate-of-rise of recovery voltage du/dt is primarily affected by the value of R_{trv} [14]. The du/dt is calculated as the discrete gradient between the voltage 4 µs after CZ and zero-crossing of voltage.

In this work, the experiments are conducted with $Z_s = 112\ \Omega$, which would correspond to a quarter-pole test. Table 1 lists the key parameters along with the CIC component values. The first set of columns identifies the objective of each experiment and its label Q<n>. The second column group lists the desired input conditions and constraints, with U_c serving as the primary control variable. The last column set presents the corresponding feasible CIC component configurations that meet the design targets.

Additionally, experiments F0 and F1 were conducted under full-pole configuration and were done to evaluate the influence of high-current amplitude, while keeping i_{peak} of the CIC close to 2.5 kA. The variation in HC amplitude was easily implemented by adjusting the charging voltage of C_{hc} and the trigger

time of SW_{hc}, without requiring any modifications to the circuit.

2.3. Experiment Approach and Performance Indicators

The interruption performance is quantified using parameters within the CZ window with the most important one being the di/dt corresponding to 50% interruption probability referred to as 'interruption limit'. Due to the occurrence of hot-dielectric reignitions, there are 2 categories of interruption limits: the thermal interruption limit, which considers only thermal failures, and overall interruption limit that accounts for overall interruption outcomes irrespective of the reignition mechanism. In order to estimate the interruption limit, a minimum of 5 interruption tests were performed at each di/dt (a controllable parameter) within a range to cover 0 to 100% of success rate. A Gaussian cumulative distribution function (CDF) was then fitted to the updated success rates and the mean of this fitted distribution represents the interruption limit.

The measured quantities from the interruption tests hold information about the interruption performance, referred to as performance indicators. The ones that are discussed in this work are $G200$ and $G500$, the arc conductance 200 ns and 500 ns before CZ, respectively, and extinction peak voltage (U_{peak}) defined as the maximum arc voltage reached shortly before CZ. Logistic regression is used to determine the mean threshold of these indicators which are called critical limits. Moreover, a modified Pearson's correlation coefficient is used to evaluate the association of all the indicators with the interruption outcome.

3. Results and Discussions

A comprehensive summary of all experiments is presented in Table 2, discussing the key performance indicator limits like G200, G500, dG/dt and U_{peak} along with their respective correlation coefficients $\bar{r}$. Except for the interruption limits, the limits of the remaining quantities are derived based on their thermal performance, i.e., distinguishing thermal failures from other outcomes. It is observed that arc conductance and voltage levels before CZ are similar for successes and hot-dielectric failures. This indicates that these outcomes are predominantly governed by the post-CZ TRV stress. Consequently, analyzing the overall interruption performance yields weak correlation and limited insight. The following subsections provide a detailed comparison of various experiments.

3.1. Influence of high current peak

The sensitivity check of the 'high current' phase was conducted as part of a full-pole experiment campaign, i.e., Z_{s} =450 Ω. In this campaign, F0 and F1 were tested at HC amplitudes of 1.9 kA (general set value) and 5.4 kA while keeping the CIC i_{peak} close to 2.5 kA. It is worth noting that the sample size of F1 was

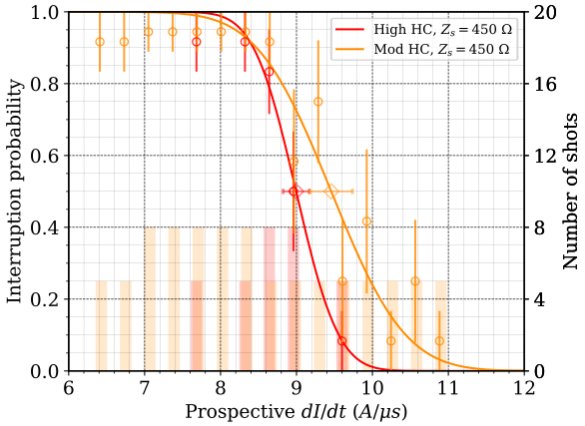

Figure 4. Comparison between thermal interruption limits at moderate (F0) and high HC (F1) experiments with data points (circles) and number of tests (bar chart). Limit values are similar with overlapping 2-σ intervals.

significantly smaller than that of F0 due to rapid nozzle ablation.

Similar overall interruption limits resulted from F0 and F1 whereas the thermal interruption limits (as shown in Fig 4) showed slight variation with overlapping 2-σ intervals; consistent with higher arc conductance limits in F1. However, the weak correlation between arc conductance-related indicators and thermal interruption outcomes reduced the confidence in this limit as a precise indicator in case of F1. Extinction peak voltage limit values remained identical.

At full-pole configuration, HC amplitudes equivalent to $(1/10)^{th}$ and $(1/4)^{th}$ of the full short-circuit current- 100% of the 50 Hz short-circuit current corresponding to 6.4 A/μs (lowest tested di/dt)- in F0 and F1, respectively, were applied. It can be inferred that the high-current (HC) amplitude — which peaks ∼6 ms before CZ — has no significant influence on the CZ conditions. This observation is in accordance with the extrapolated experimental findings of [6], who investigated the effect of HC amplitude in interruption tests in SF_6. Their measurements at various current levels, ranging from 25% to 100% of the full short-circuit current (11 kA to 51 kA peak), showed the same thermal recovery speed, hence, CZ conditions. Leveraging the finding that the pressure build-up in our experimental CB is independent of HC phase (no back-heating), tests were performed at low HC amplitudes to minimize nozzle wear. Interruption performance at HC amplitudes > 5 kA has not been tested.

3.2. Influence of injection current peak

An injection current 20% higher than the moderate setting of 2.6 kA was applied, maintaining the same current profile over the last 130 μs at a di/dt of 16 A/μs (linear at least over the last 4 μs before CZ). The applied TRV waveforms were identical for both exper-

		HC quantities		CIC quantities					CIC output components				
Aim	Name	i_{hc}^{peak} kA	$\frac{T_{hc}}{2}$ ms	U_c kV	i_{ic}^{peak} kA	$\frac{di}{dt}$ A/µs	u_{trv}^{peak} kV	$\frac{du}{dt}$ kV/µs	L_{ic} mH	C_{ic} µF	R_{trv} Ω	C_{trv} nF	$\frac{T_{ic}}{4}$ µs
Moderate IC,TRV	Q0	1.9	12.5	25	2.6	15.7	30	1.7	1.4	16.8	110	100	240
High IC	Q1	1.9	12.5	25	3.4	15.6	30	1.7	1.4	30	115	100	330
High TRV	Q2	1.9	12.5	30	2.6	15.8	36	1.7	1.7	13.2	110	100	240
Moderate HC	F0	1.9	12.5	30	2.4	9.5	34	4.2	2.8	21.4	430.5	9.8	770
High HC	F1	5.4	10.5	28	2.3	8.9	33	4.0	2.8	21.4	430.5	9.8	770

Table 1. Current injection circuit components for various quarter-pole tests (Z_s=112 Ω in CO_2 /O_2 mixture)

Z_s Ω	Name	N	Interruption Limit overall A/µs value	σ_μ	σ	thermal A/µs value	σ_μ	σ	$G200$ mS [$\bar{r}$]	$G500$ mS [$\bar{r}$]	dG/dt mS/µs [$\bar{r}$]	U_{peak} V [$\bar{r}$]
112	Q0	54	16.29	0.16	1.3	16.69	0.18	1.3	3.8 [-0.804]	7.7 [-0.831]	12.4 [-0.785]	717 [0.638]
112	Q1	55	15.06	0.20	1.4	15.31	0.16	1.2	4.6 [-0.617]	8.7 [-0.671]	13.5 [-0.669]	677 [0.499]
112	Q2	40	15.64	0.16	1.0	16.11	0.16	1.1	3.9 [-0.704]	7.5 [-0.705]	12.1 [-0.626]	754 [0.480]
450	F0	90	8.23	0.31	1.0	9.44	0.17	0.8	0.24 [-0.67]	0.55 [-0.71]	1.01 [-0.73]	1062 [0.65]
450	F1	31	8.17	0.12	0.7	9.0	0.08	0.4	0.6 [-0.484]	1.5 [-0.534]	3.3 [-0.500]	1090 [0.571]

Table 2. Comparison of limit values of interruption performance indicators at various stresses in full-pole and quarter-pole configurations.

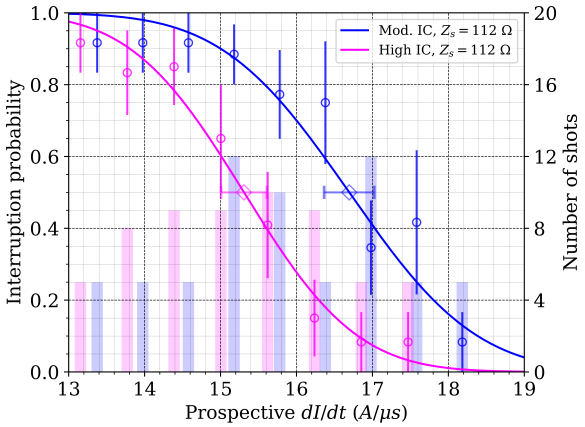

Figure 5. Comparison between thermal interruption limits at moderate (Q0) and high IC (Q1) experiments with data points (circles) and number of tests (bar chart). A clear reduction in the Q1 limit can be observed, pertaining to accumulated heat before CZ

iments at a given RRRV. ∼50 shots were performed for each condition.

In the higher injection current experiment (Q1), a thermal interruption limit of (15.31 ± 0.16) A/µs was observed, representing an 8% decrease compared to the moderate quarter-pole test (Q0) as shown in Fig 5. A larger proportion of failures in Q1 were identified as thermal reignitions at the same di/dt

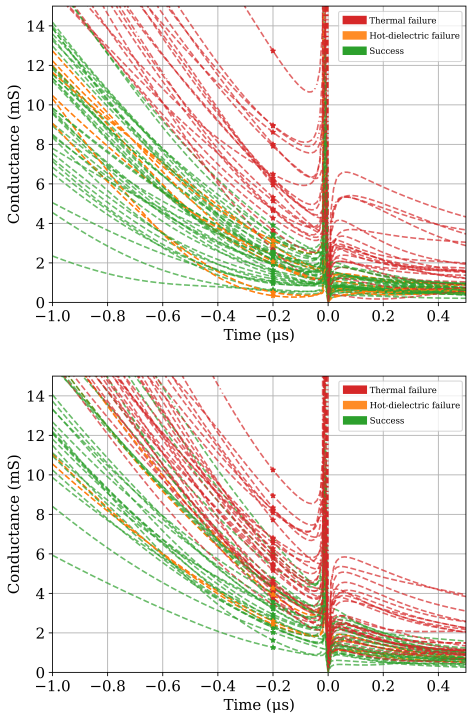

Figure 6. Arc conductance decay plots in experiments at moderate, Q0 (top) and high IC, Q1 (bottom), highlighting larger G200 values (astericks) in Q1

setting whereas Q0 exhibited more significant hot-dielectric failures under similar conditions. This shift in failure mechanism led to a reduction in the thermal interruption limit. As a result, the overall interruption limit and the thermal limit in Q1 became closely aligned.

Fig 6 presents the arc conductance plots during the final 1 µs before CZ. In case of Q1, both higher conductances and faster decay rates can be observed along with smaller scatter among individual curves, however, Q0 exhibits clearer separation between thermal successes and failures. The resulting arc conductance limits in Q1 were marginally higher than Q0, with G200 and G500 limit values for former being 4.6 m S and 8.7 m S while the extinction peak voltage limits remained comparable at 717 V in Q0 with a 5% decrease in Q1.

Weaker thermal interruption performance is observed in Q1, implying possible differences in the CZ conditions in terms of heat exchange. In the synthetic testing guide by *Hochrainer*, it is recommended to maintain the injection current same as the short-circuit current for at least the last 100 µs [15]. However, this standardized time window might have been employed considering SF_6-the primary switching medium, which largely differs from CO_2 in terms of thermodynamic properties. SF_6 possess lower values of ρC_p at temperatures above 4000 K (onset of conduction) which aids in losing energy quickly before CZ [16, 17], thus, requiring less time for voltage to adapt to current decay (smaller arc time constants). This might not be true for CO_2 based on the conclusions of this work. A potential reason could be that CO_2 exhibit a peak in ρC_p at 7000 K obstructing the heat loss through radial conduction- the dominant cooling mechanism at low currents < 100 A. So, if IC decays from a higher level, this energy (to be dissipated at CZ) is higher for Q1 as compared to Q0. This might suggest that the IC should follow the short-circuit current for a longer duration before CZ in order to closely mimic the CZ conditions in CO_2-based mixtures. A similar 100 µs time window requirement was inferred from *Slepian*'s theoretical work which proposed an arc constriction time constant of ∼50 µs. This theory was later validated experimentally by *Frind et al* in *air* who demonstrated that a 30 µs window of correct $\mathrm{d}i/\mathrm{d}t$ is sufficient, allowing up to 10% of deviation from linearity [3]. It is to be noted that this test was performed at a blow pressure of ∼30 bar whereas 10.8 bar is maintained in our experiment setup. Although it is adequate to induce sonic conditions at the nozzle throat, it possibly leads to inadequate axial convective cooling.

Another important parameter is the nozzle material which, in case of typically-used PTFE, release fluorine compounds and/or species which help in recovering the electric strength when ablated at high currents. The use of PMMA nozzle in this work nonetheless rules out this mild aid in arc cooling; might leading to deterioration in thermal recovery.

3.3. Influence of TRV peak

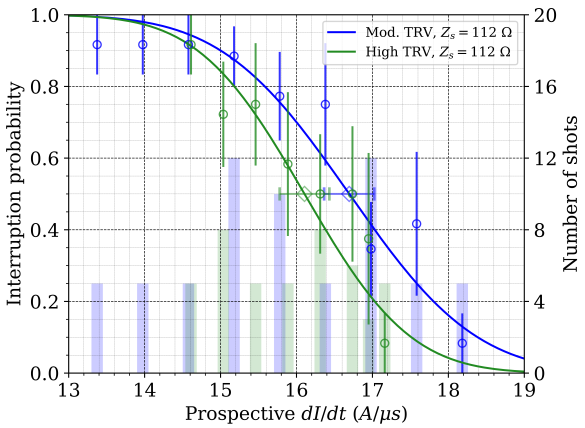

Figure 7. Comparison between thermal interruption limits at moderate (Q0) and high TRV (Q2) experiments with data points (circles) and number of tests (bar chart). No change in the limits for the tested TRV peak range.

The quarter-pole test series Q2 was conducted under a higher TRV peak of 36 kV at $\mathrm{d}i/\mathrm{d}t$ of ∼16 A/µs as shown in Fig 2, representing a 17% increase compared to Q0. The thermal and overall interruption limits were found to be 16.11 A/µs and 15.64 A/µs, respectively, with a standard deviation of 1–2%. These values fall within the uncertainty intervals of the corresponding limits in Q0 indicated in Fig 7.

Similar conductance-related limits were observed, with G200 and G500 values of 3.9 m S and 7.5 m S, respectively. However, the extinction peak voltage limit was approximately 5% higher than that recorded in Q0.

Q2 introduces significant changes in the TRV waveform 10 - 15 µs after current zero, as shown in Fig 2. This test was conducted to investigate the influence of this time window on interruption outcomes, particularly in cases of successful interruption and hot-dielectric failure. The thermal interruption performance — characterized by the thermal limit and thermal arc conductance limits — remains practically unchanged between Q0 and Q2. This suggests that the variations in TRV peak do not affect thermal failure mechanisms.

4. Conclusions

Thermal interruption tests are performed in blown arcs of CO_2 /O_2 (90% / 10%) gas mixture in a puffer-type circuit breaker using a synthetic circuit. The aim is to understand the influence of synthetic circuit stresses in 3 distinct phases on the interruption performance, whose conclusions are listed as follows:

- High-current phase: An increase of HC peak from 2 kA to 5 kA was implemented to study the influence

of current levels 5 ms before CZ, i.e. significantly prior to CZ. The results indicated no effect on the thermal interruption performance.

- Injection current phase: The aim was to investigate the effect of the synthetic test current >100 µs before CZ. This was achieved by increasing the peak injection current from 2.6 kA to 3.4 kA while maintaining the same current decay profile as short-circuit current in the last 100 µs and 170 µs respectively. A deterioration in thermal interruption performance was observed at the higher current level, as indicated by lower $\mathrm{d}i/\mathrm{d}t$ limits and G200 values. This indicates that the accumulated heat in the arcing region continues to be present beyond CZ, suggesting that the IC should follow the short-circuit current for a longer duration before CZ in order to closely mimic the CZ conditions in CO_2-based mixtures. This recommendation holds valid for convection-stabilized arcs near CZ with minimal effect of back-heating- a condition that potentially differs from the standardized synthetic tests on HV breakers, where the HC amplitude is at least an order of magnitude higher than in this work.
- Transient recovery phase: Furthermore, experiments were conducted to study the influence of voltage 10-15 µs *after* CZ. The TRV peak was increased from 30 kV to 36 kV keeping the $\mathrm{d}u/\mathrm{d}t$ same after CZ. For the tested TRV and RRRV range, the thermal recovery showcased no effect of TRV peak.

Next steps involve conducting experiments at CIC current levels below the 2.5 kA range, to probe the hypothesis that thermal interruption performance would improve due to lower current levels prior to the 100 µs window before CZ.

Acknowledgements

We would like to extend our gratitude to Hitachi Energy Limited for funding this project. Also thanks to Martin Seeger and Joseph Engelbrecht from Hitachi Energy Research Centre in Baden-Dättwil for their valuable feedback.

References

[1] *High-voltage switchgear and controlgear - Part 100: Alternating-current circuit-breakers*. CH, 2021. URL: https://webstore.iec.ch/en/publication/62785.

[2] IEC 62271-101: High-voltage switchgear and controlgear – Part 101: Synthetic testing of high-voltage alternating current circuit-breakers, 2012. Standard.

[3] G. Frind. *Experimental Investigation of Limiting Curves for Current Interruption of Gas Blast Breakers*. Springer US, Boston, MA, 1978. ISBN 978-1-4757-1685-6. doi:10.1007/978-1-4757-1685-6_3.

[4] T. Uchii et al. Thermal interruption capability of carbon dioxide in a puffer-type circuit breaker utilizing polymer ablation. In *IEEE/PES Transmission and Distribution Conference and Exhibition*, volume 3, pages 1750–1754 vol.3, 2002.

[5] B. Radisavljevic et al. Switching Performance of Alternative Gaseous Mixtures in High-Voltage Circuit Breakers. In *The 20th International Symposium on High Voltage Engineering, Buenos Aires, Argentina*, 2017.

[6] H. Nishikawa, A. Kobayashi, T. Okazaki, and S. Yamashita. Arc extinction performance of sf_6 gas blast interrupter. *IEEE Transactions on Power Apparatus and Systems*, 95(6):1834–1844, 1976. doi:10.1109/T-PAS.1976.32284.

[7] C. Franck et al. Comparative test program framework for non-SF_6 switching gases. *B&H Electrical Engineering*, 15:23–30, 2021.

[8] P. Pietrzak, M. Perret, M. Boening, et al. Wear of the arcing contacts and gas under free burning arc in SF_6 alternatives. *IEEE Transactions on Power Delivery*, 38(3):2133–2140, 2023. doi:10.1109/TPWRD.2023.3234364.

[9] J. Engelbrecht et al. Statistical methods for identifying small differences in the thermal interruption performance of SF_6 alternatives. *Plasma Physics and Technology*, 10(1):36–39, 2023. doi:10.14311/ppt.2023.1.36.

[10] P. Pietrzak, J. T. Engelbrecht, D. Kumari, and C. M. Franck. Short-line fault interruption performance comparison of sf_6 alternatives. *IEEE Transactions on Power Delivery*, 39(6):3071–3081, 2024. doi:10.1109/TPWRD.2024.3451178.

[11] J. T. Engelbrecht, D. Kumari, P. Pietrzak, and C. M. Franck. Thermal current interruption in CO_2-based mixtures part I: Evaluating parameter dependence. *Journal of Physics D: Applied Physics*, 58(22):225503, 2025. doi:10.1088/1361-6463/adcf33.

[12] J. T. Engelbrecht, D. Kumari, and C. M. Franck. Thermal current interruption in CO_2-based mixtures part II: Influence of flow conditions. *Journal of Physics D: Applied Physics*, 58(22):225504, 2025. doi:10.1088/1361-6463/adcf32.

[13] M. Muratovic, J. T. Engelbrecht, P. Simka, et al. An experimental circuit breaker for benchmarking the intrinsic interruption performance of SF_6 alternative gas mixtures. *IEEE Transactions on Power Delivery*, 39(6):3082–3091, 2024. doi:10.1109/TPWRD.2024.3451235.

[14] W. P. Legros, A. M. Genon, M. M. Morant, et al. Computer aided design of synthetic test circuits for high voltage circuit-breakers. *IEEE Power Engineering Review*, 9(4):63–64, 1989. doi:10.1109/MPER.1989.4310602.

[15] A. Hochrainer. Synthetic testing for high power circuit-breakers. Electra Report ELT 006-1, CIGRE, 1968.

[16] J. Liu, Q. Zhang, J. D. Yan, et al. Analysis of the characteristics of dc nozzle arcs in air and guidance for the search of sf_6 replacement gas. *Journal of Physics D: Applied Physics*, 49(43):435201, 2016. doi:10.1088/0022-3727/49/43/435201.

[17] L. Zhong, J. Wang, J. Xu, et al. Effects of buffer gases on plasma properties and arc decaying characteristics of c_4f_7n–n_2 and c_4f_7n–co_2 arc plasmas. *Plasma Chemistry and Plasma Processing*, 39(6):1379–1396, 2019. doi:10.1007/s11090-019-10015-8.